Solar Energy 263 (2023) 111934

Contents lists available at ScienceDirect

Solar Energy

journal homepage: www.elsevier.com/locate/solener

Application of the novel satellite calibrated method "Radiative Forcing Meter" on a high albedo test facility for CO_2 compensation

Federico Rossi [a], Beatrice Castellani [b,*], Aron Pazzaglia [c], Alessia Di Giuseppe [c], Stefania Bonafoni [d], Mirko Filipponi [e], Andrea Presciutti [f], Franco Cotana [b]

[a] Department of Engineering, CIRAF, University of Perugia, Perugia, Italy
[b] Department of Engineering, CIRIAF, University of Perugia, Perugia, Italy
[c] CIRIAF, Interuniversity Research Center on Environment and Pollution "M.Felli", University of Perugia, Perugia, Italy
[d] Department of Engineering, University of Perugia, Perugia, Italy
[e] School of Science and Technology, University of Camerino, Camerino, Italy
[f] Dep. of Economy, Universitas Mercatorum, Rome, Italy

ARTICLE INFO

Keywords:
Albedo
Global warming
Radiative forcing meter
Emission credit

ABSTRACT

The increase of terrestrial albedo may be considered a key strategy to mitigate global warming, since it produces a reduction of the radiative forcing (RF). The RF concept, as defined by IPCC, is used in literature for calculations of the CO_2 compensation due to albedo increase, which can be achieved by the development of high-albedo solutions (cool materials, *retro*-reflective materials, green infrastructures, etc.). The authors have previously proposed a new procedure, called RF-meter, to measure the continuous time history of the RF due to an albedo increase ($RF_{\Delta\alpha}$) and so to calculate the related CO_2 offset potential by high-albedo solutions. RF-meter procedure is based on the continuous albedo measurements at ground level and discrete satellite calibration. The proposed method is tested on a high-albedo surface (HAS) of 900 m^2 treated with a high-reflective paint installed on the roof of CIRIAF building, University of Perugia, Italy. The experimental field is equipped with an albedometer, a weather station and a Calculus Unit. The measured data are elaborated by the Calculus Unit to calculate the RF time history and the compensated CO_2. Data from albedo monitoring exhibited that albedo of HAS was always higher than albedo before the treatment (α_0) and the average $\Delta\alpha$ is equal to 0.3. The calibration procedure allows to reduce the errors on $RF\Delta_\alpha$ calculation. The maximum difference between albedo values from albedometer and satellite measurements resulted equal to 3.9%. Results from the Calculus Unit showed an amount of CO_2 compensated by HAS equal to 73 kg_{CO2eq}/m^2.

1. Introduction

Increasing frequency and severity of weather and extreme climate events (i.e. extreme precipitation, droughts, tropical cyclones, fire weather, etc.) are direct consequence of the ongoing Global Warming (GW). As stated in IPCC (International Panel on Climatic Change) 6th Report [13], "it is unequivocal" that human activities are responsible for more than 50% of the change in the atmosphere over the industrial time. During the decade 2010–2019 total Greenhouse Gas (GHG) emission from human activities continued to grow and was higher than any previous time in human history, resulting equal to 59 $GtCO_2eq$ in 2019 (i.e. 12% higher than in 2010 and 54% higher than in 1990). The energy sector is responsible for 34% of global GHG emissions in 2019, followed by industry (24%), agriculture (22%), transport (15%) and buildings (5.6%) [16]. GHG emissions, aerosols, solar radiation, land use, and albedo are the main drivers of GW [18].

The influence of a climate driver is evaluated by Radiative Forcing (RF) concept by IPCC definition [14]. In addition to the already known strategies to mitigate GW such as renewables energies, energy efficiency and Carbon Capture and Sequestration (CCS) [10,11,8,7], the increase of terrestrial albedo may represent a key strategy that need to be further investigated [15]. In fact, albedo plays an important role on Earth

* Corresponding author.
E-mail addresses: federico.rossi@unipg.it (F. Rossi), beatrice.castellani@unipg.it (B. Castellani), aron.pazzaglia@studenti.unipg.it (A. Pazzaglia), alessia.digiuseppe@crbnet.it (A. Di Giuseppe), stefania.bonafoni@unipg.it (S. Bonafoni), mirko.filipponi@unipg.it (M. Filipponi), andrea.presciutti@unimercatorum.it (A. Presciutti), franco.cotana@unipg.it (F. Cotana).

https://doi.org/10.1016/j.solener.2023.111934
Received 7 March 2023; Received in revised form 31 July 2023; Accepted 2 August 2023
Available online 15 August 2023

thermal balance and on global temperature and may be involved both in adaptation (i.e. Urban Heat Island and indoor thermal comfort improvement) and mitigation strategies (i.e. CO_2 offset): an increase on terrestrial albedo produces a reduction on RF. The increase of terrestrial albedo may be reached via High-Albedo Solutions (HAS) which involve cool materials, *retro*-reflective materials, green infrastructures, etc. and they represent a promising pathway to counteract GW.

The relationship between the management of terrestrial albedo by HAS and GW mitigation has been largely considered in literature: different models have been proposed by involving the RF concept for CO_2 offset calculation, as reported in [27].

A simplified method, called Emissions Equivalent of Shortwave Forcing (EESF), was introduced by [4] and relates RF due to an albedo change ($RF_{\Delta\alpha}$) to the RF following a constant in time change of CO_2 concentration. Results obtained from different authors using the metric EESF are consistent and within a range of 1.3–3.3 kg CO_{2eq}/m^2 for a $\Delta\alpha = 0.01$ [4,1,26,28].

A time-dependent metric, called Time-Dependent Emissions Equivalence (TDEE), was also proposed in [6] to consider the time dependency of CO_2 removal processes. Similar to TDEE is the Global Warming Potential (GWP) metric, where the $RF_{\Delta\alpha}$ is evaluated over a discretized time horizon and it is then normalized to the RF following a unit pulse CO_2 emission accumulated over the same time horizon [29,25]. For a time horizon of 100 years, the values of GWP (1.4 kg CO_{2eq}/m^2) are consistent to that obtained by EESF.

However, literature proposals do not involve several aspects such as albedo change ($\Delta\alpha$) as a function of location features (i.e. latitude and longitude) and of time variation, climatic conditions (i.e. atmospheric absorption on downward and upward beams), and time variation of previous parameters.

Under this framework, a new procedure, called RF-meter, which overtakes the literature penalties have been presented by the Authors [27] to measure the continuous time history of the RF$\Delta\alpha$ and so to calculate the related CO_2 offset potential by HAS. HAS produce an increase of RF and so they could represent an alternative and valid method to tackle GW. No similar experimental research based on this methodology can be found in literature. RF-meter procedure is based on continuous albedo measurements at ground level, satellite calibration, and precise evaluation of RF, taking into account variations in solar, atmospheric and superficial parameters. Such dependences are crucial for the precise evaluation of the compensated CO_2. In fact, the continuous albedo measurements allow to measure RF time history; moreover, Sentinel-2 with a high spatial resolution of 10–60 m and 2–3 days revisit time at mid-latitude, is chosen for periodically satellite measurements, ensuring a better estimation of RF$\Delta\alpha$. RF-meter procedure allows to assess CO_2 offset by albedo change with the following characteristics: accuracy (measurement based RF estimation), localization, meteo climatic conditions, and satellite calibration. Since a reliable method is available, it is proposed to introduce HAS into an ETS (Emission Trading Scheme).

It is common in literature that satellite measurements, or parameters estimated from satellite measurements, are validated with ground measurements. The method for albedo retrieval from Sentinel-2 proposed in this work was already tested in [5] with ground-based measurements in two different environments (rural and urban), proving to be reliable and accurate (root mean square error of 0.02). As a matter of fact, the calculation of the RF of a given surface, which is a necessary parameter to determine CO_2 compensation in accordance with the IPCC framework, requires the precise evaluation of the solar irradiation at the top of the atmosphere (W_{TOA}) as well as the solar irradiation which exits from the top of the atmosphere (W_{out}).

The authors in [27] have already given a detailed description of the RF-meter methodology, the explanation of the reasons for integrating on-ground and satellite measurements, satellite characteristics, and just a preliminary example of the calibration procedure, based on a single satellite acquisition. The present research contribution instead comes after a period of experimental campaign during which both the on-ground measurements and multiple satellite acquisitions (in different days) were acquired and analyzed, giving the first results of the practical application of the RF-meter procedure to a high albedo surface over a significant period of time. An important part of this stage of the research is the development of the calculus unit based on the discretization by finite time of the proposed model. The results constitute a breakthrough in the topic.

In addition, the experimental campaign gave the authors the opportunity also to evaluate some critical issues resulting from the model implementation and largely discussed in the present paper. The evaluation of the emerged critical issues has set the framework for a dedicated experimental investigation, currently ongoing.

Specifically, the proposed method is tested on a HAS of 900 m^2 treated with a high-reflective paint supplied by Watergy International and installed on the roof of CIRIAF building, University of Perugia, Italy. The experimental field is equipped by an albedometer, a weather station, and a Calculus Unit. The measured data are elaborated by code to calculate the RF time history and the compensated CO_2. Preliminary results of the proposed method applied on the designed experimental field are reported in this study. To the best of our knowledge, there is no previous similar experimental research, adopting the described procedure, in literature.

2. Materials and methods

The present paper investigates the application of the *RFmeter* procedure, proposed in [27], to an HAS, installed on the roof of CIRIAF building, University of Perugia, Italy, according to the steps shown in Fig. 1.

The objective is assessing the effect of HAS in terms of CO_2 compensation. The procedure starts with changing the albedo of a surface (called HAS in Fig. 1), through the application of high-albedo materials on it. To do so, an experimental field is developed and equipped with ground instruments for in-continuo measurements of the incident radiation (W_{in}), the reflected radiation and its albedo during the day. Albedo is the ratio of upwelling to downwelling radiative flux at the surface. Downwelling flux, i.e. the solar irradiance reaching the surface, is the sum of a direct component and a diffuse component, therefore having an hemispherical geometry. Following the definition in [20], black-sky albedo is defined as albedo in the absence of a diffuse component, i.e. coming from the direct sun beam direction, and is a function of solar zenith angle. White-sky albedo is defined as albedo in the absence of a direct component when the diffuse component is isotropic. In this work we have measured the so called blue-sky albedo, i.e. the combined sum of the direct and diffuse solar irradiance components at a specific solar zenith angle defined by the day and time of the measurement sampling.

Under cloudless conditions, the diffuse irradiance is on the order of 15–20% of the global hemispherical irradiance [23]. Far from sunrise and sunset, the direct irradiance is about 300–400 W/m^2 higher than the diffuse one.

For measured earth's surface reflectance quantities made from satellite, the estimated albedo is again the blue-sky albedo, therefore depending on the solar zenith angle for the presence of the direct sun beam component.

To calculate the RF, it is necessary also to calculate the incident radiation at the top of the atmosphere (W_{TOA}) and this is done by astronomical equations:

$$RF_{\Delta\alpha} = -\frac{W_{in}^{\ 2}}{W_{TOA}}\cdot\Delta\alpha = -W_{in}\cdot T_a\cdot\Delta\alpha \quad (1)$$

where T_a is the solar energy transmission coefficient due to the atmosphere. RF$\Delta\alpha$ is therefore assessed by a mixed procedure made of measured and calculated quantities. The RF$\Delta\alpha$ values, coming from Eq.

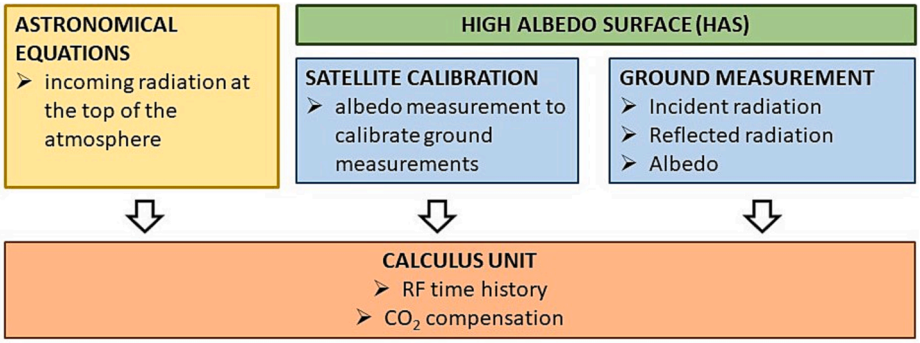

Fig. 1. RFmeter flowchart.

(1), are then calibrated to reduce errors by discrete satellite measurements, according to a proprietary algorithm [5].

The satellite used is the Sentinel-2, a multispectral imaging mission comprising two identical polar-orbiting satellites (Sentinel-2A and Sentinel-2B) placed in the same sun-synchronous orbit at a mean altitude of 786 km, phased at 180° to each other, with a high revisit time (2–3 days at mid-latitudes). A multi-spectral instrument (MSI) onboard measures the Earth's reflected radiance in 13 spectral bands in the visible, (VIS), near-infrared (NIR) and shortwave infrared (SWIR) spectral range, at different spatial resolutions ranging from 10 to 60 m on the ground [12]. Surface reflectance is obtained by applying an atmospheric correction to TOA reflectance product, described in [3]. In [5], a narrow-to-broadband conversion method was used to estimate surface albedo from the surface reflectivity measurements of the multispectral sensor onboard Sentinel-2. The total solar radiation signal measured by a satellite sensor observing the earth's surface consists of three main components [2]:

1. Solar radiation scattered from the sun beam into the sensor Field of View (FOV), called "atmospheric path radiation". Such radiation has not reached the surface, but it is scattered in the air volume between ground and satellite;
2. The direct and diffuse (global) solar radiation reflected from the target surface and entering in the sensor FOV, directly transmitted through the atmosphere (so, affected by the atmospheric transmittance and scattering);
3. The so-called "adjacency effect", representing the reflected background radiation scattered by the air volume into the sensor FOV and the radiation backscattered by the atmosphere to the surface

Only solar radiation component n. 2 contains information from the target surface reflectance: the other components have to be estimated and removed from the total sensor measurement, as usually performed in atmospheric correction of satellite imagery [17]. The path radiance decreases with wavelength. It is usually very small for wavelengths greater than 800 nm. The influence of the adjacency effect also decreases with wavelength and is very small for spectral bands beyond 1.5 μm [24].

Concerning the observations from Sentinel-2, different level products are available for users: in this work Level-2A products providing Surface Reflectances (SR) were used for albedo retrieval. Level-2A data are radiometrically and geometrically corrected, including orthorectification, projected into the UTM-WGS 84 coordinate system. SR for each Sentinel-2 band, used to compute the broadband albedo as in [5], are atmospherically corrected as described on ESA (European Space Agency) portal [12]. The atmospheric correction of Sentinel-2 SR includes the correction of the scattering of air molecules (Rayleigh scattering), of the absorbing and scattering effects of atmospheric gases, in particular ozone, oxygen and water vapour, and the correction of absorption and scattering due to aerosol particles. For each scene, an aerosol optical thickness map and a water vapour map are also generated in the Leve2-2A data, useful to estimate the main atmospheric parameters influencing the values of path radiance, transmittance, and global radiance. Effectively, atmospheric correction of Sentinel-2 data is performed in the processor "Sen2Cor" using a set of look-up tables (LUTs) generated via a library for radiative transfer, i.e. a collection of functions and programs for calculation of solar and thermal radiation in the Earth's atmosphere. The LUTs are generated for a wide variety of atmospheric conditions, solar geometries, and ground elevations, and are calculated with a spectral resolution of 0.6 nm. This database is subsequently resampled with the Sentinel-2 spectral responses, in order to obtain the sensor-specific functions needed for the atmospheric corrections.

The quality of SR products after atmospheric correction was assessed in literature; for instance, by comparing corrected data obtained from Sentinel-2 imagery with field spectrometry data [30].

The results proved the accuracy of the applied atmospheric corrections, with coefficients of determination higher than 0.90 and a relative error in surface reflectance of only 2–3%.

The formulation of SR with the specific transmittance contribution, in the framework of the overall atmospheric correction detailed above, is reported in [9]. An error of about 10% on transmittance (quite a big error considering the reliability of LUTs on Sen2Cor) leads to a variation of about 8% on SR in the optical band.

The calibration by Sentinel-2 is carried out, correcting the Eq. (1) with a calibration factor k_i, defined as the ratio between the albedo measured by satellite at i-th passage and the ground continuous albedo measure, as in Eq. (2).

$$RF_{\Delta\alpha} = k_i \cdot W_{in} \cdot T_a \cdot \Delta\alpha \tag{2}$$

So, the uncertainty of the RF calculation depends on satellite data (k_i), on-ground albedometer (W_{in} and $\Delta\alpha$) and on the evaluation of T_a. The albedo retrieval from Sentinel-2 has a root mean square error of 0.02, as in [5].

Therefore, data from satellite observations, ground measurements and astronomical equations are elaborated by a calculus unit, to determine the CO_2 compensated by the HAS in accordance with Eq. (3).

$$CO_{2,\,comp} = \frac{\sum_{i=1}^{N} \int_{T_i}^{T_{i+1}} \mathrm{S} \cdot RF_{\Delta\alpha,i}(t) \cdot dt}{\int_0^T A_E \cdot k_r \cdot y_r(t) \cdot dt} \tag{3}$$

where T_i and T_{i+1} are time values at i-th and (i + 1)-th passages of satellite, N are the numbers of satellite passages during T, *S* is the area of the HAS, A_E is the Earth surface, k_r is the radiative efficiency of CO_2 and $y_r(t)$ is the time-dependent decay in abundance of CO_2 following an instantaneous release of it at time t = 0. Eq. (3) is obtained extending the *GWP* concept by IPCC and considering the effect of albedo change in terms of equivalent CO_2. The detailed discussion of the model is in [27].

2.1. Experimental facility

An experimental facility is developed, treating a part of the flat roof of CIRIAF building, Department of Engineering, University of Perugia (43° 7′ 9.449″ N, 12° 21′ 27.451″ E) with a high-reflective paint, to apply the RF*meter* procedure for the calculation of the compensated CO_2. The used high-reflective white paint is the Cool Barrier Roof Optimum supplied by Watergy International Group. The technical datasheet of the high-reflective paint is provided in Table 1.The HAS covers 900 m^2 to ensure reliable satellite measurements, since the resolution of Sentinel-2 is a 10 m × 10m pixel.

Fig. 2 shows an aerial view of the HAS and the roof before and after the treatment.

The HAS is equipped with the following instruments:

- An albedometer (A), located in the HAS orthocenter (model LP PYRA 05 Delta OHM srl) connected to a data logger (model HD35EDWH-NRE Delta OHM srl);
- A weather station (WS) located on the roof of CIRIAF building;
- Two type T thermocouple probes (TC – positioned in a part of the flat roof without treatment and TC_{HAS} – positioned in the HAS) connected to a temperature datalogger (12 channels Temperature Recorder LT Lutron BTM-4208SD datalogger).

The albedometer is made by two pyranometers (class 1) in accordance with ISO 9060:2018. It was positioned in the HAS orthocenter at 0.5 m, in accordance with ASTM E1918-06. Data sheet of the albedometer is presented in Table 2.

The albedometer was connected to a data logger for albedo monitoring. The data logger was set to record albedo values every 30 s. Data sheet of the data logger is presented in Table 3 below. The solar radiation and albedo were measured in accordance with ASTM-E1918-06 [19].

A fixed weather station was used to perform the environmental monitoring. The station consists of (i) a thermohygrometer sensor, (ii) a pyranometer upward oriented, (iii) a direction and speed anemometer, (iv) a direct radiometer, with sunshine duration sensor, and (v) a rain gauge. All the sensors perform a continuous monitoring campaign collecting average data every 10 min [19]. Data concerning global radiation (W/m^2), and direct radiation (W/m^2) were collected during the monitoring campaign, and then used in the data post-processing stage.

The surface temperature of the two configurations (i.e. HAS and roof without treatment) was monitored by two type T thermocouples, TC_{HAS} and TC respectively, connected to a 12 channels Temperature Recorder LT Lutron BTM-4208SD datalogger. Features and specifications of the Temperature Recorder and type T thermocouple probes are listed in Table 4.

The measured data were then elaborated by a Calculus Unit to determine the RF time-history and the compensated CO_2 over a T horizon. The Calculus Unit is described in the Paragraph 2.2.

Table 1
Product data sheet of Cool Barrier Roof Optimum paint supplied by Watergy International Group.

Cool Barrier Roof Optimum paint	
TECHNICAL FEATURES	**SPECIFICATIONS**
Product Description	Super durable, cold-liquid applied membrane, one-component, seamless, water-based, highly elastic and UV-stable, aliphatic polyurethane, designed to provide easy application and a durable waterproofing solution
Colour	Traffic white (RAL 9016)
Solar Reflectance Index	≥ 100 (RAL 9016)
Density	~1.30 kg/l (23 °C) (EN ISO 2811-1)
Solid content	~63.4% by weight ~52.0% by volume
Shelf life	9 months from date of production
Storage conditions	The product must be stored properly in original, unopened, and undamaged sealed packaging in dry conditions at temperature between 0 °C and +25 °C

2.2. Description of the Calculus unit

A VBA computational code has been developed to calculate RF and CO_2 offset with Eq. (2) and (3) discretized by finite time Δt. A user-friendly VBA interface (Control panel) has been developed to facilitate data entry and display (Fig. 3).

The Control Panel and then the code consists of 4 sections:

1. Data Section for acquisition external data input;
2. Setting Section for data setting as constants and parameters;
3. Satellite Section for Satellite data entry;
4. Calculation Section for performing calculation and display results.

In the Data Section of control panel, the operator can acquire data input from the albedometer such as the incident Radiation (W_{in}), the reflected radiation (W_{out}) and the albedo (α_{HAS}). A "LOAD" button (Fig. 3) allows to select the file CSV data source where the albedometer records solar data. Once the operator chooses the starting and the ending time to analyze, the "EXTRACT" button allows to select just the data inside the chosen range (Fig. 3, the green and red squares) as data input of the computational code. In detail the input of code is the matrix (N,4) where N is the number of the acquisitions (time step: 30 s) and 4 is the number of parameters recorded for i-th acquisition: A_Date_i; $W_{in,i}$, $W_{out,i}$, $\alpha_{HAS,i}$.

In the Setting section the operator can set parameters and constants for RF and CO_2 offset determination such as A_E, HAS and k_r. The operator can choose if leave or change these parameters.

In the Satellite section the operator can insert date and hour (S_Date_j) and the albedo values ($\alpha_{SAT,j}$) obtained by j-th satellite passage. This data is employed as input in the code for the albedo calibration and CO_2 offset determination. In detail, in the satellite section the operator can edit a table where the j-th row is the j-th Satellite passage and the column are the relative acquired data (S_Date_j, $\alpha_{SAT,j}$). From a computational point of view, the code builds a matrix (m,2) where m is the number of satellite passages.

Pushing the "CALC" Button in Calculation section the operator can run the code and see the main results such as CO_2 offset and RF value relative to the last acquisition of albedo. Main outputs can be reported on the table in excel page.

The code employs the Eqs. (2) and (3), discretized by finite time. The code consists in two subroutines: i) *Ta_Subrutine* for Ta determination; ii) *CO_2_Subrutine* for CO_2 offset determination.

Ta_subrutine is employed for $T_{a,i}$ determination (the solar energy transmission coefficient) relative to i-th solar data acquisition at i-th acquisition time. As $T_{a,i}$ depends on $W_{TOA,i}$, the code calculates $W_{TOA,i}$ relatives to each i-th acquisition time by astronomical formulas. In detail $W_{TOA,i}$ depends just on data and hour (A_Date_i) and on geographical coordinates (latitude and longitude).

a) *CO_2_Subrutine*

The first step of this subroutine is the $RF\Delta_{\alpha,i}$ determination for each i-th acquisition by Eq. (4):

$$RF_{\Delta\alpha,i} = k_j \cdot W_{in,i} \cdot T_{a,i} \cdot (\alpha_{HAS,i} - \alpha_{0,i}) \quad (4)$$

where $k_j = \alpha_{HAS,i}/\alpha_{SAT,i}$ if A_Date_i is equal to S_Date_j and it keeps constant until A_Date_i is equal to S_Date_{j+1} when $k_{j+1} = \alpha_{HAS,i}/\alpha_{SAT,j+1}$.

The second step is the CO_2 offset determination by Eq. (5) discretized by finite time Δt:

Fig. 2. An aerial view of the test facility at CIRIAF (University of Perugia) with the shape of the equipment (i.e. A, WS, TC, and TC_{HAS}) evidenced in red (Fig. 1a); surface under test before albedo change (Fig. 1b); surface under test after albedo change (Fig. 1c). (For interpretation of the references to color in this figure legend, the reader is referred to the web version of this article.)

Table 2
Technical features of the albedometer LP PYRA 05 (Technical features are referred to the pyranometers which make up the albedometer LP PYRA 05).

Albedometer	
TECHNICAL FEATURES	**SPECIFICATIONS**
Model	LP PYRA 05
Sensor	Thermopile
Typical sensitivity	10 W/m^2
Measuring range	0 ÷ 2000 W/m^2
Viewing angle	2π sr
Spectral range (50%)	305 nm ÷ 2800 nm
Spectral error	<0.5%
Operating temperature	−40 °C ÷ 80 °C

$$CO_{2,\,comp} = \frac{\mathrm{HAS}\sum_{i=1}^{N} RF_{\Delta\alpha,i}\cdot\Delta t}{A_E K_r \sum_{i=1}^{N} y_{r,i}\cdot\Delta t} \tag{5}$$

where A_E, k_r and HAS are the constants set on the panel control and Δt is the acquisition time step (30 sec).

3. Critical issues resulting from the model implementation

The implementation of the model in the calculus unit has highlighted two issues related to the correct choice of the input data. The first issue is related to the calculation of the transmission coefficient due to the atmosphere, T_a, defined as in Eq. (6) [27]:

$$T_a = \frac{W_{in}}{W_{TOA}} \tag{6}$$

where W_{TOA} is the solar radiation per unit area at the top of the atmosphere (calculated through astronomical equations) and W_{in} is the solar radiation per unit area which hits the HAS (measured on ground).

When the solar elevation angle is low, the Eq. (6) results in values of T_a bigger than 1. This result is due to the contribution of the atmospheric diffraction and diffusion included in the measurement of W_{in} by the upper pyranometer of the albedometer.

Table 3
Data sheet of the data connected to the albedometer.

Data logger	
TECHNICAL FEATURES	**SPECIFICATIONS**
Product description	Waterproof wireless data logger with custom LCD display and internal antenna
Housing	Polycarbonate
Protection degree	IP 67
Operating temperature and humidity conditions	−20…+70 °C / 0…100%RH
Logging interval	5,10,15,30 s / 1,2,5,10,15,30,60 min

Table 4
Technical features of the 12 channels Temperature Recorder LT Lutron BTM-4208SD with type T thermocouple probes.

Datalogger	
TECHNICAL FEATURES	**SPECIFICATIONS**
Model	Lutron BTM-4208SD 12 channels
Sampling time	1–3600 s
Resolution	0.1 °C/1 °C, 0.1 °F/1 °F
Operating temperature	0 ÷ 50 °C
Operating humidity	Less than 85% R.H.
Thermocouples	
TECHNICAL FEATURES	**SPECIFICATIONS**
Type	T
Length	30 m
Temperature range	−50 ÷ 250 °C
Accuracy Class	1
Sheath material	AISI316

A correction in the calculus unit was made, using in Eq. (6) the measurement of the only direct radiation that hits the HAS, by the sensors mounted on the weather station. In the future, the albedometer will be complemented by a pyrheliometer, which will measure only the direct incident radiation for the correct estimation of T_a.

The second issue is the determination of the albedo change $\Delta\alpha$, as the difference between the albedo of the HAS (α_{HAS}) and the albedo before the treatment (α_o): also α_o is a time dependent parameter (daily and seasonal). The assessment of α_o is fundamental for the determination of the correct value of $\Delta\alpha$ and $RF_{\Delta\alpha}$, and for the quantifications of the amount of CO_2 compensated, especially if the HAS is introduced as a method to get emission credits in the ETS system.

The evolution of the $\Delta\alpha$ over time needs to be continuously monitored by the simultaneous measurement of both α_o and α_{HAS}, with the objective of finding an eventual correlation between the two profiles, but, most of all, a standardized and shared procedure for the evaluation of both $\Delta\alpha$ and $RF_{\Delta\alpha}$.

This will be done in a dedicated experimental investigation, planned for the next months. For the purposes of the present paper, the authors used daily αo values recorded before the roof treatment, as discussed in Paragraph 4.

4. Results and discussion

The following section shows the results of superficial temperature and albedo monitoring and albedo calibration. Specifically, data from 20th August to 30th August 2022 were taken into account.

4.1. Superficial temperature analysis

Two type T thermocouples connected to a temperature datalogger were used for superficial temperature monitoring in the two field configurations (i.e. TC_{HAS} and TC for the high albedo roof and roof without treatment, respectively). TC_{HAS} and TC were positioned as shown in Fig. 2.

Results concerning the superficial temperature monitoring from 20th August to 30th August 2022 were shown in Fig. 4. The superficial temperature values followed a sinusoidal trend and were always lower in the high-albedo configuration than in the roof without treatment in all selected days. In particular, roof without treatment exhibited higher temperature than HAS in the middle of the day.

Fig. 5 shows the ΔT values, defined as the difference between the HAS superficial temperature and the superficial temperature of the roof without treatment. The highest ΔT value resulted equal to 9.7 °C for the 21st, 25th and 29th of August during the warmest hours of the day, specifically at 3p.m., 2:30p.m., and 3:30p.m. respectively. The lowest ΔT values were found during the night for all selected days. In particular, the minimum ΔT value resulted equal to 0.9 °C during night (from 3 a.m. to 7 a.m.) for the 28th of August.

The cooling effect of high-albedo treatments in terms of superficial temperature has already been demonstrated by the Authors both through experimental campaigns ([21]) and simulation model ([22]).

In Fig. 6, a representative day (i.e. 23th of August 2022) of the considered period was shown. A sinusoidal trend was evidenced for both scenarios. The reference case exhibited greater fluctuations during the day with respect to the enhanced scenario, especially in the hottest hours of the day. The maximum ΔT value was found equal to 9.1 °C at 3:20 p.m whilst the lowest ΔT value resulted equal to 1.9 °C during the early hours.

The superficial temperature monitoring highlights the cooling effect of high-albedo treatments on buildings' surfaces, which is highest in the hotter part of day but is conserved also at night. This demonstrates the crucial role of albedo in adaptation strategies to counteract global warming.

4.2. Albedo analysis

An albedometer made by two pyranometers (Class 1) was used for albedo monitoring during the experimental campaign. The albedometer was connected to a data logger which was set to record data every 30 s.

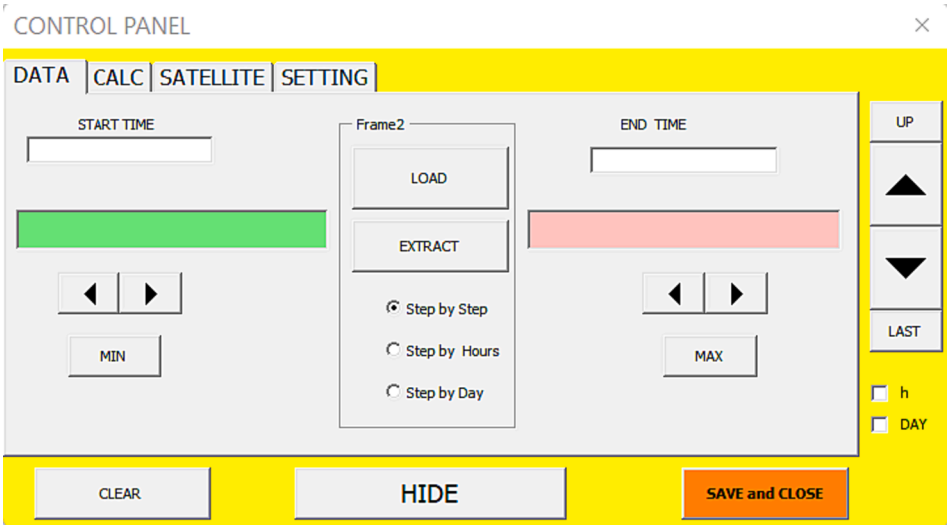

Fig. 3. Control panel interface (Data section).

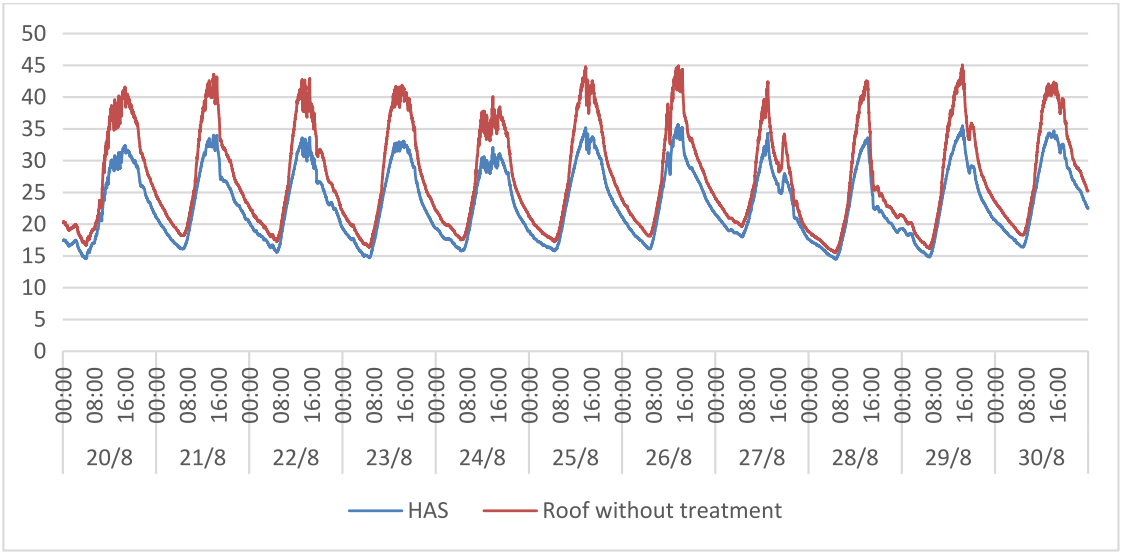

Fig. 4. Superficial temperature monitoring from 20th August to 30th August 2022.

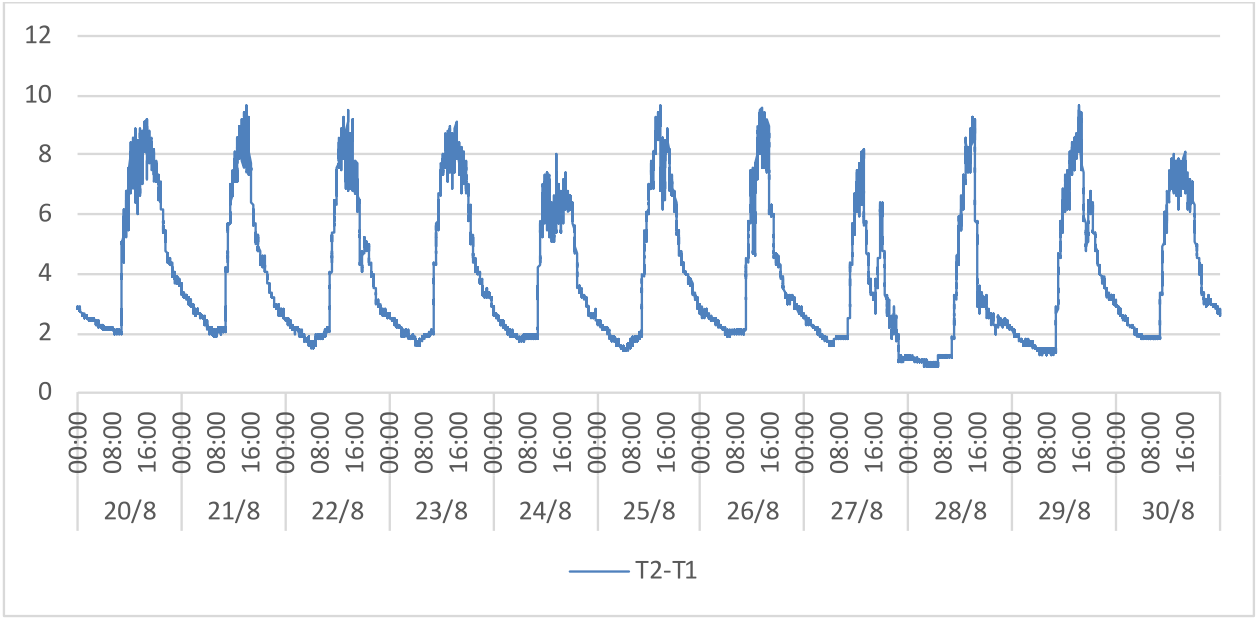

Fig. 5. Temperature differences between the HAS (T1) and the roof without treatment (T2).

The albedo (α) was calculated as the ratio between the incident radiation (W_{in}) and the reflected radiation (W_{ref}) by both the two configurations investigated.

Albedo values vary throughout the day, as shown in Fig. 7 which describes the albedo variation for the 30th of August 2022 from 8 a.m. to 5:30p.m. The daily trend showed that the albedo in the HAS ranged between 62% and 87% for the 30th of August.

In Fig. 8 below, a significant difference between albedo values before and after albedo change by HAS was shown. The 13th of May 2022 and the 19th of May 2022 were used to show the albedo variation before and after albedo change by HAS, respectively, from 2p.m. to 4p.m. The daily profile before treatment is similar on the different days monitored and the 13th of May is the most representative. Therefore, the 13th of May was chosen as the reference case for α_0, resulting that the average value of $\Delta\alpha$ is equal to 0.3.

Before the albedo change, data concerning albedo monitoring for the 13th of May 2022 varied from 53% to 56% whilst after albedo change by HAS on the 19th of May 2022, the albedo values ranged from 84% to 88%.

4.3. Satellite calibration and evaluation of the CO_2 compensated

The satellite calibration was carried out, considering satellite data related to the following days: 23rd, 26th and 28th of August 2022. Sentinel-2 passed over the HAS at 12 a.m. of each day. Fig. 9 shows the albedo maps from Sentinel-2 above the HAS in the three days. The HAS is highlighted by the white square. The colored bar on the right indicates albedo values from 0 to 1. The deep blue color corresponds to 0 while the red color is 1. In particular, the pixels over the HAS are yellow and orange corresponding to albedo values equal to about 0.80. The roof part without treatment is green showing an albedo equal to about 0.50.

A comparison between the albedo values, measured on ground, and the albedo values by satellite are reported in Fig. 10. There is a slight difference between the two values in the different days: in the 23rd is

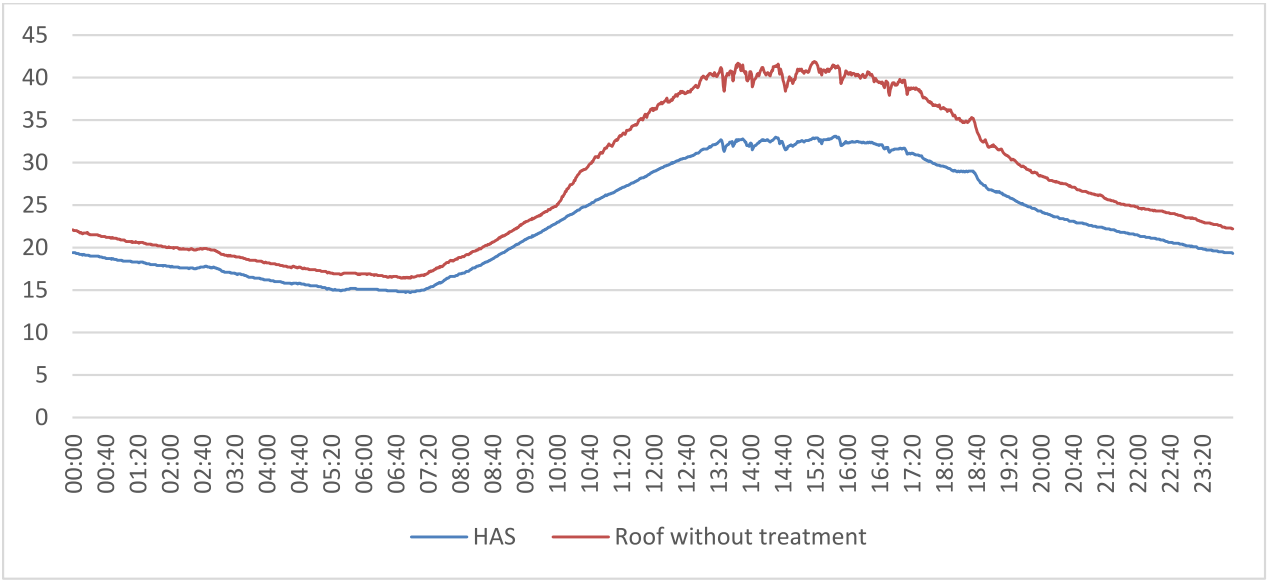

Fig. 6. Superficial temperature monitoring during the 23th of August 2022.

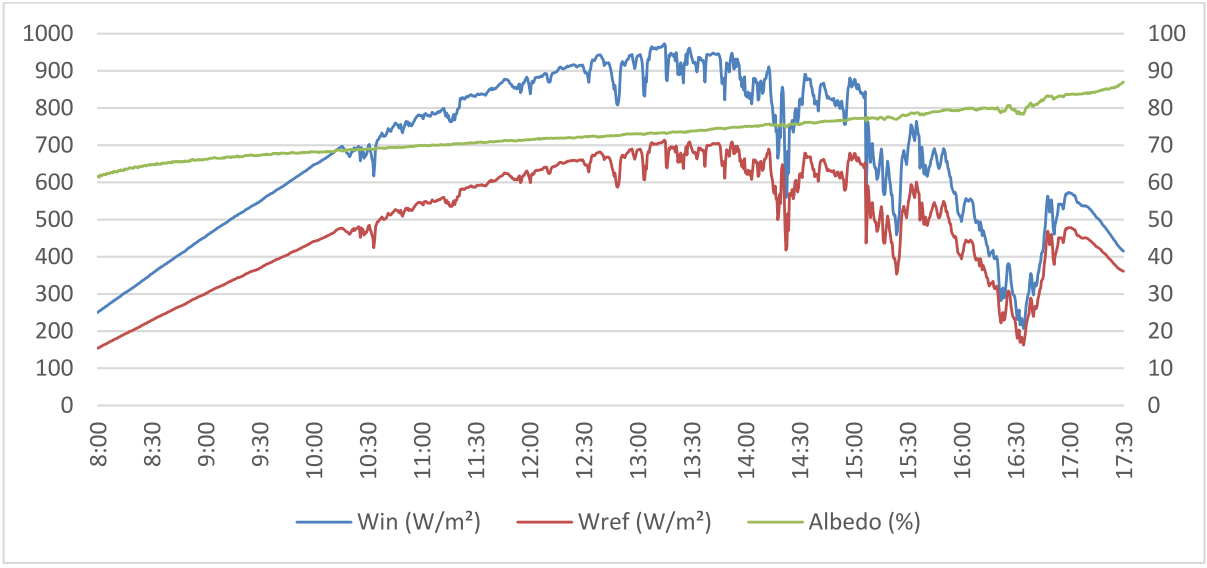

Fig. 7. Albedo, W_{in}, W_{ref} values for the 30th of August 2022.

−3.6%; in the 26th is 3%; in the 28th is −3.9%.

The calibration constant k_i is determined as in Table 5.

So, four albedo values are used to calculate $RF\Delta_\alpha$: α_{HAS} (t_i) in the first period (20–23 August); α_{HAS} (t_i) corrected with a calibration factor of 0.950 in the second period (23–26 August); α_{HAS} (t_i) corrected with a calibration factor of 1.042 in the third period (26–28 August); α_{HAS} (t_i) corrected with a calibration factor of 0.945 in the last one (28–30 August).

Results concerning albedo monitoring from ground measurements and the albedo values corrected by a calibration procedure were shown in Figs. 11, 12, and 13, for the 23rd of August, 26th of August, and 28th of August, respectively. The calibration procedure was carried out by occasional satellite measurements on HAS, reducing the affection of errors on $RF\Delta_\alpha$ calculation [27].

Fig. 11 shows that albedo values ranged from 72% to 89% by ground measurements during the 23rd of August 2022 from 12 a.m. to 5:30p.m.; after calibration procedure, the albedo values varied from 68% to 84% during the considered period.

Fig. 12 shows that albedo values ranged from 63% to 77% by ground measurements during the 26th of August 2022 from 8 a.m. to 5:30p.m.; after satellite measurements, the albedo values varied from 59% to 67% from 8 a.m. to 12 a.m. and from 74% to 80% from 12 a.m. to 5:30p.m.

Fig. 13 shows that albedo values ranged from 56% to 74% by ground measurements during the 28th of August 2022 from 8 a.m. to 5:30p.m.; after satellite measurements, the albedo values varied from 58% to 74% from 8 a.m. to 12 a.m. and from 67% to 70% from 12 a.m. to 5:30p.m.

The measured data are then elaborated by Calculus Unit to calculate the RF time history and the compensated CO_2. Results from the Calculus Unit showed an amount of CO_2 compensated by HAS equal to 73 kg_{CO2eq}/m^2. This value, corresponding to 2.43 kg_{CO2eq}/m^2 for $\Delta\alpha = 0.01$, is consistent with literature data, varying in the range 1.3–3.3 kg_{CO2eq}/m^2 for a $\Delta\alpha = 0.01$ using EESF method [4,1,26,28].

5. Conclusion

The present paper concerns the application of the RF-meter

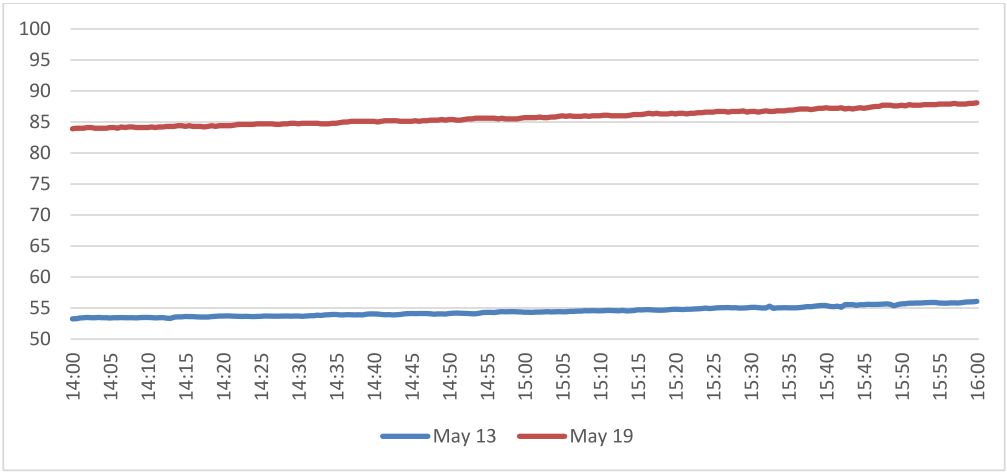

Fig. 8. Albedo monitoring after and before albedo change by HAS.

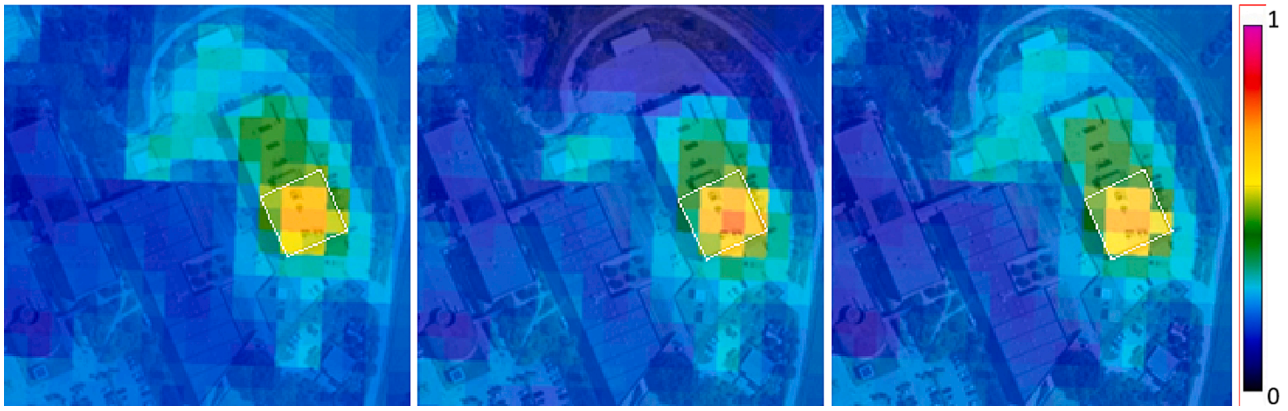

Fig. 9. Albedo map from Sentinel-2 satellite – 23rd, 26th and 28th of 28 August 2022.

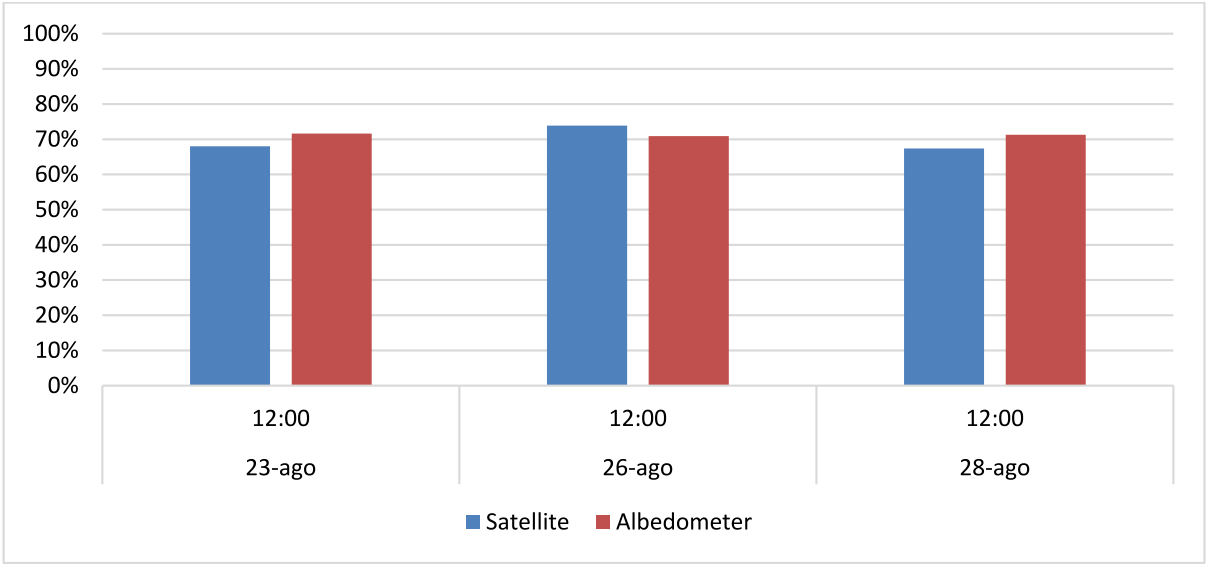

Fig. 10. Different albedo values from satellite and albedometer.

procedure to a High-Albedo Surface (HAS) for the quantification of the amount of CO_2 compensated. The authors have previously developed the above-mentioned RF-meter procedure for the determination of the radiative forcing (RF) time-history and the compensated CO_2 by a superficial albedo change.

The procedure is here applied to an experimental facility developed treating a part of the flat roof of CIRIAF building, Department of Engineering, University of Perugia with a high-reflective paint. The RF-meter

Table 5
Calibration constant k_i obtained as the ratio between the albedo values from albedometer and satellite.

Day	Albedo(Satellite measurement)	Albedo(Albedometermeasurement)	Calibration factor k_i
23 Aug	68.0%	71.6%	0.950
26 Aug	73.9%	70.9%	1.042
28 Aug	67.4%	71.3%	0.945

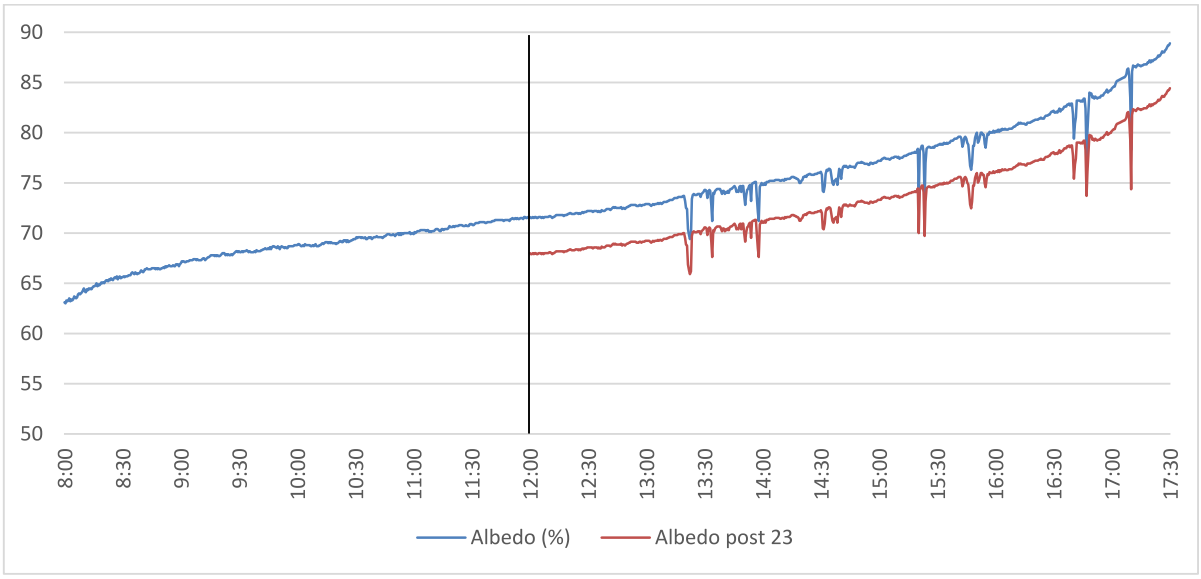

Fig. 11. Albedo calibration for the 23rd of August 2022.

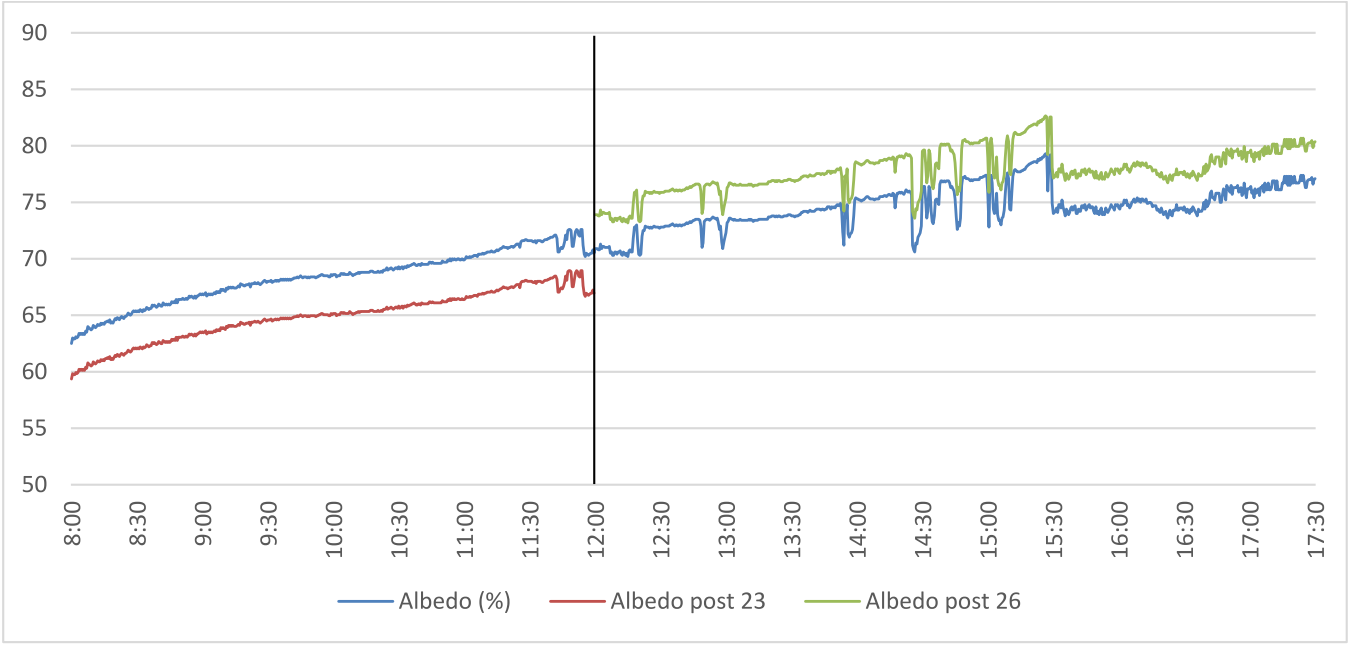

Fig. 12. Albedo calibration for the 26th of August 2022.

procedure foresees ground equipment and satellite calibration for the albedo measurement and the development of a calculus unit for the calculation of the RF due to the albedo increase and CO_2 compensation.

The experimental facility is equipped with an albedometer, a weather station and superficial thermocouples. The satellite used is the Sentinel-2, with an image resolution of 10mx10m, and the calibration is carried out, introducing a calibration factor, defined as the ratio between the albedo measured by satellite at its passage and the ground continuous albedo measure.

The calculus unit is constituted by a VBA computational code for the discretized calculation of the radiative forcing due to the albedo increase and CO_2 offset. Results from the Calculus Unit showed an amount of CO_2

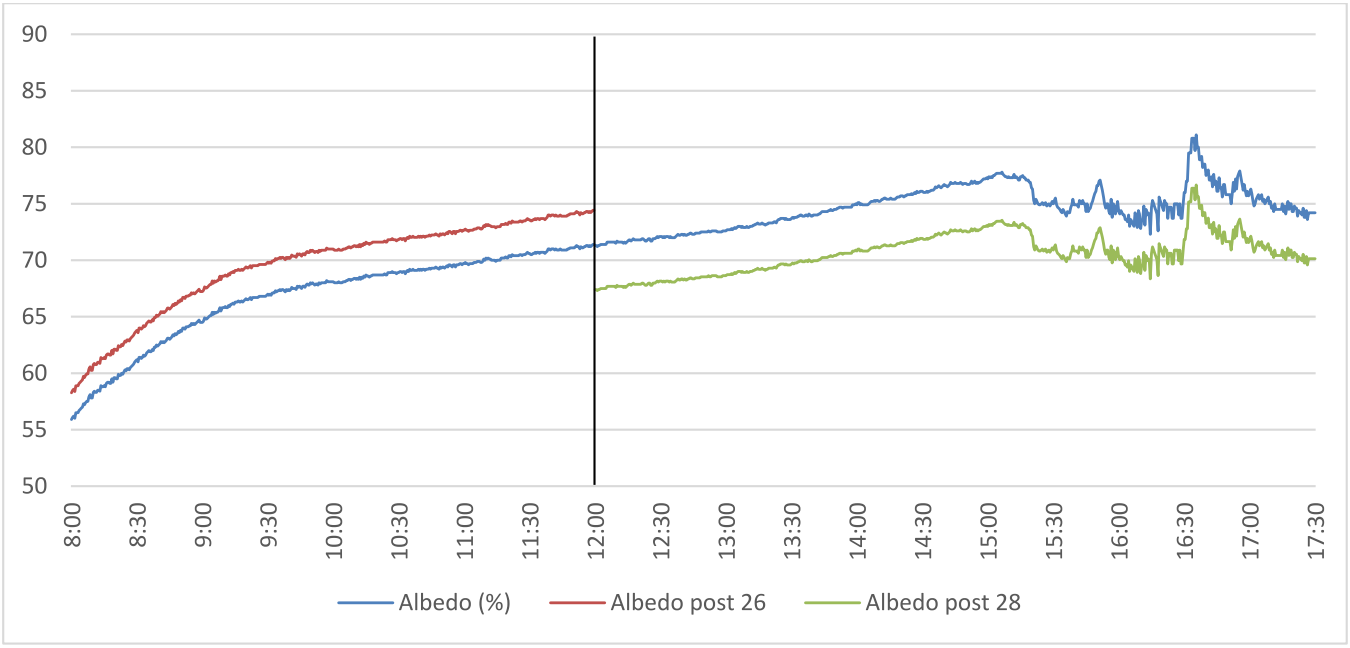

Fig. 13. Albedo calibration for the 28th of August 2022.

compensated by HAS equal to 73 kg_{CO2eq}/m^2.

Results from the experimental investigation are summarized hereunder:

- The superficial temperature values followed a sinusoidal trend and were always lower in the enhanced configuration (HAS) than on the roof without treatment during the monitored period, particularly during the warmest hours of day. The highest ΔT value resulted equal to 9.7 °C for the 21st, 25th and 29th of August at 3p.m., 2:30p.m., and 3:30p.m., respectively.
- A significant difference between albedo values before and after albedo change by HAS was found and Δα resulted an average equal to 0.3.
- The calibration procedure carried out by occasional satellite measurements on HAS, allowed to reduce the affection of errors on $RF\Delta_\alpha$ calculation. The maximum difference between albedo values from albedometer and satellite measurements resulted equal to 3.9%.

The uncertainty of the estimation of the results depends not only on the difference between albedo values but also on the value of T_a. As reported in the work, this value was determined empirically, highlighting the relative criticalities. The aim of the next research activities will be to determine T_a with specific instruments (pyranometer). Only by knowing the measurements of two albedometers and the pyranometer, it will be possible to estimate the uncertainty of the results.

The development of the calculus unit has highlighted two important issues, which will be further investigated in the future. The first one is related to the atmosphere transmission coefficient, which results bigger than 1 when the solar elevation angle is low. This is due to the contribution of the atmospheric diffraction and diffusion included in the measurement of the incident radiation by the upper pyranometer of the albedometer. So, a correction in the calculus unit was made, using the measurement of the only direct radiation that hits the surface, by the sensors mounted on the weather station. In the future, a pyrheliometer, which will measure only the direct incident radiation, will be installed in the experimental facility and values will be monitored for a larger period.

The second issue is the determination of the albedo change Δα, as the difference between the albedo of the HAS and the albedo before the treatment (α_o), which is also a time dependent parameter (daily and seasonal). The assessment of α_o is fundamental for the determination of the correct value of the albedo increase and the related radiative forcing, especially if the albedo increase is introduced as a method to get emission credits in the ETS system. The investigation on the proper procedure for the evaluation of α_o is planned for the next months. The results presented in this paper constitute the first application of the RF-meter procedure to a high-albedo surface and add new knowledge in the pathway of the recognition of high-albedo solutions as a strategy to reinforce Emission credit system and tackle global warming.

The planned future studies are due to make the RF-meter an objective and precise tool, which may be used to assign credits to high-albedo solutions in the frame of the ETS system.

CRediT authorship contribution statement

Federico Rossi: Conceptualization, Methodology, Validation, Writing – review & editing, Supervision, Project administration. **Beatrice Castellani:** Conceptualization, Methodology, Validation, Investigation, Data curation, Writing – original draft, Writing – review & editing, Visualization, Supervision. **Aron Pazzaglia:** Investigation, Data curation, Writing – original draft, Visualization. **Alessia Di Giuseppe:** Investigation, Data curation, Writing – original draft. **Stefania Bonafoni:** Resources, Data curation, Writing – review & editing. **Mirko Filipponi:** Formal analysis, Investigation. **Andrea Presciutti:** Software, Formal analysis, Investigation, Resources, Data curation, Writing – original draft. **Franco Cotana:** Supervision, Project administration.

Declaration of Competing Interest

The authors declare that they have no known competing financial interests or personal relationships that could have appeared to influence the work reported in this paper.

References

[1] Akbari, H., Menon, S., Rosenfeld, A., 2009. Global cooling: increasing world-wide urban albedos to offset CO2. Clim. Change 94 (3-4), 275–286.
[2] Asrar, G., 1989. Theory and Applications of Optical Remote Sensing. J. Wiley, New York.

[3] ASTM-E1918-06; Standard Test Method for Measuring Solar Reflectance of Horizontal and Low-Sloped Surfaces in the Field. ASTM International, ASTM: West Conshohocken, PA, USA, 2015, pp. 1–3.

[4] Betts, R.A., 2000. Offset of the potential carbon sink from boreal forestation by decreases in surface albedo. Nature 2000 (408), 187–190.

[5] Bonafoni, S., Sekertekin, A., 2020. Albedo retrieval from Sentinel-2 by new narrow-to-broadband conversion coefficients. IEEE Geosci. Remote Sens. Lett. 17 (9), 1618–1622. https://doi.org/10.1109/LGRS.2020.2967085.

[6] Bright, R.M., Bogren, W., Bernier, P., Astrup, R., 2016. Carbon equivalent metrics for albedo changes in land management contexts: Relevance of the time dimension. Ecol. Appl. 26 (6), 1868–1880.

[7] Castellani, B., Morini, E., Bonamente, E., Rossi, F., 2017. Experimental investigation and energy considerations on hydrate-based biogas upgrading with CO2 valorization. Biomass Bioenergy 105, 364–372.

[8] Castellani, B., Gambelli, A.M., Nicolini, A., Rossi, F., 2019. Energy and environmental analysis of membrane-based CH4-CO2 replacement processes in natural gas hydrates. Energies 12, 850.

[9] Chavez, P.S., 1996. Image-based atmospheric correction—Revisited and improved. Photogramm. Eng. Remote Sens. 62 (9), 1025–1036.

[10] Cotana, F., Rossi, F., Nicolini, A., 2011. Evaluation and optimization of an innovative low-cost photovoltaic solar concentrator. Int. J. Photoenergy 2011, 1–10.

[11] de Santoli, L., Lo Basso, G., Bruschi, D., 2014. Hybrid system with an integrated CHP plant fueled by H2NG blends: Theoretical energy-environmental analysis and foreseeable optimizations. Energ. Build. 71, 88–94.

[12] ESA, The European Space Agency, available online at https://sentinel.esa.int/web/sentinel/user-guides/sentinel-2-msi/processing-levels/level-2 (accessed on 31/07/2023).

[13] IPCC, 2021a: Climate Change 2021: The Physical Science Basis. Contribution of Working Group I to the Sixth Assessment Report of the Intergovernmental Panel on Climate Change [Masson-Delmotte, V., P. Zhai, A. Pirani, S.L. Connors, C. Péan, S. Berger, N. Caud, Y. Chen, L. Goldfarb, M.I. Gomis, M. Huang, K. Leitzell, E. Lonnoy, J.B.R. Matthews, T.K. Maycock, T. Waterfield, O. Yelekçi, R. Yu, and B. Zhou (eds.)]. Cambridge University Press, Cambridge, United Kingdom and New York, NY, USA, 2391 pp. https://doi.org/10.1017/9781009157896.

[14] IPCC, 2021b: Annex VII: Glossary [Matthews, J.B.R., V. Möller, R. van Diemen, J.S. Fuglestvedt, V. MassonDelmotte, C. Méndez, S. Semenov, A. Reisinger (eds.)]. In Climate Change 2021: The Physical Science Basis. Contribution of Working Group I to the Sixth Assessment Report of the Intergovernmental Panel on Climate Change [Masson-Delmotte, V., P. Zhai, A. Pirani, S.L. Connors, C. Péan, S. Berger, N. Caud, Y. Chen, L. Goldfarb, M.I. Gomis, M. Huang, K. Leitzell, E. Lonnoy, J.B.R. Matthews, T.K. Maycock, T. Waterfield, O. Yelekçi, R. Yu, and B. Zhou (eds.)]. Cambridge University Press, Cambridge, United Kingdom and New York, NY, USA, pp. 2215–2256, https://doi.org/10.1017/9781009157896.022.

[15] IPCC, 2021c: Summary for Policymakers. In: Climate Change 2021: The Physical Science Basis. Contribution of Working Group I to the Sixth Assessment Report of the Intergovernmental Panel on Climate Change [Masson Delmotte, V., P. Zhai, A. Pirani, S.L. Connors, C. Péan, S. Berger, N. Caud, Y. Chen, L. Goldfarb, M.I. Gomis, M. Huang, K. Leitzell, E. Lonnoy, J.B.R. Matthews, T.K. Maycock, T. Waterfield, O. Yelekçi, R. Yu, and B. Zhou (eds.)]. Cambridge University Press, Cambridge, United Kingdom and New York, NY, USA, pp. 3–32, https://doi.org/10.1017/9781009157896.001.

[16] IPCC, 2022: Climate Change 2022: Mitigation of Climate Change. Contribution of Working Group III to the Sixth Assessment Report of the Intergovernmental Panel on Climate Change [P.R. Shukla, J. Skea, R. Slade, A. Al Khourdajie, R. van Diemen, D. McCollum, M. Pathak, S. Some, P. Vyas, R. Fradera, M. Belkacemi, A. Hasija, G. Lisboa, S. Luz, J. Malley, (eds.)]. Cambridge University Press, Cambridge, UK and New York, NY, USA. https://doi.org/10.1017/9781009157926.

[17] Kaufman, Y.J., 1985. The atmospheric effect on the separability of field classes measured from satellites. Remote Sens. Envir. 18 (1), 21–34.

[18] S.K. Gulev, P.W. Thorne, J. Ahn, F.J. Dentener, C.M. Domingues, S. Gerland, D. Gong, D.S. Kaufman, H.C. Nnamchi, J. Quaas, J.A. Rivera, S. Sathyendranath, S.L. Smith, B. Trewin, K. von Schuckmann, R.S. Vose, Changing State of the Climate System. In Climate Change 2021: The Physical Science Basis. Contribution of Working Group I to the Sixth Assessment Report of the Intergovernmental Panel on Climate Change [MassonDelmotte, V., P. Zhai, A. Pirani, S.L. Connors, C. Péan, S. Berger, N. Caud, Y. Chen, L. Goldfarb, M.I. Gomis, M. Huang, K. Leitzell, E. Lonnoy, J.B.R. Matthews, T.K. Maycock, T. Waterfield, O. Yelekçi, R. Yu, and B. Zhou (eds.)]. Cambridge University Press, Cambridge, United Kingdom and New York, NY, USA, 2021, pp. 287–422, https://doi.org/10.1017/9781009157896.004.

[19] Pisello, A.L., Cotana, F., Nicolini, A., Buratti, C., 2014. Effect of dynamic characteristics of building envelope on thermal-energy performance in winter conditions: in field experiment. Energy Build. 80, 218–230.

[20] Lucht, W., Schaaf, C.B., Strahler, A.H., 2000. An algorithm for the retrieval of albedo from space using semiempirical BRDF models. IEEE Trans. Geosci. Remote Sens. 38 (2), 977–998.

[21] Morini, E., Castellani, B., De Ciantis, S., Anderini, E., Rossi, F., 2018. Planning for cooler urban canyons: Comparative analysis of the influence of façades reflective properties on urban canyon thermal behavior. Sol. Energy 162, 14–27. https://doi.org/10.1016/j.solener.2017.12.064.

[22] Morini, E., Touchaei, A., Castellani, B., Rossi, F., Cotana, F., 2016. The impact of albedo increase to mitigate the urban heat Island in Terni (Italy) Using the WRF model. Sustainability 8 (10), 999.

[23] Myers, D.R., 2012. Solar radiation resource assessment for renewable energy conversion. Comprehens. Renew. Energy 213–237.

[24] Richter, R., Schlapfer, D., 2008. Considerations on water vapor and surface reflectance retrievals for a spaceborne imaging spectrometer. IEEE Trans Geosci. Remote Sens. 46 (7), 1958–1966.

[25] Rogers, J.D., Stephens, R.D., 1988. Absolute infrared intensities for F-113 and F-114 and an assessment of their greenhouse warming potential relative to other chlorofluorocarbons. J. Geophys. Res.-Atmos. 93, 2423–2428.

[26] Rossi, F., Cotana, F., Filipponi, M., Nicolini, A., Menon, S., Rosenfeld, A., 2013. Cool roofs as a strategy to tackle Global Warming: economical and technical opportunities. Adv. Build. Energy Res. 7 (2), 254–268.

[27] Rossi, F., Filipponi, M., Castellani, B., Bonafoni, S., Ghenai, C., 2022. A novel measurement-based method for assessing global warming mitigation via high-albedo solutions. Energies 15, 5695.

[28] Sciusco, P., Chen, J., Abraha, M., Lei, C., Robertson, G.P., Lafortezza, R., Shirkey, G., Ouyang, Z., Zhang, R., John, R., 2020. Spatiotemporal variations of albedo in managed agricultural landscapes: inferences to global warming impacts (GWI). Landscape Ecol. 35 (6), 1385–1402.

[29] K. Shine, R.G. Derwent, D.J. Wuebbles, J.J. Morcrette, Radiative forcing of climate. In Climate Change: The IPCC Scientific Assessment. Cambridge University Press, New York, Melbourne, 1990.

[30] Sola, I., García-Martín, A., Sandonís-Pozo, L., Álvarez-Mozos, J., Pérez-Cabello, F., González-Audícana, M., Llovería, R.M., 2018. Assessment of atmospheric correction methods for Sentinel-2 images in Mediterranean landscapes. International Journal of Applied Earth Observation and Geoinformation 73, 63–76.